J. Fluid Mech. (2006), *vol.* 558, *pp.* 113–131. © 2006 Cambridge University Press
doi:10.1017/S002211200600992X Printed in the United Kingdom

Double-diffusive interleaving on horizontal gradients

By R. KRISHNAMURTI

Department of Oceanography and Geophysical Fluid Dynamics Institute,
Florida State University, Tallahassee, FL 32306-4360, USA

(Received 4 May 2005 and in revised form 28 November 2005)

Results are presented from laboratory experiments on lateral intrusive flows driven by horizontal gradients of properties in double-diffusive systems. These are variations on the classical experiments in which salt stratified fluid was separated from a sugar stratified fluid by a removable barrier. With the removal of this barrier, lateral intrusions of sugar solution into the salt solution alternated in the vertical with salt intrusions into the sugar solution. In our present study, the fluid has continuous horizontal gradients of sugar, density-compensated by opposing horizontal gradients of salt, rather than the discontinuity of properties in the classical experiments.

Observations of these new experiments include: shadowgraphs, PTV (particle tracking velocimetry) showing the structure of the flow, and PIV (particle-image velocimetry) from which velocity vector fields on a vertical plane were obtained; from these, mean flows, Reynolds stresses, and associated momentum fluxes were computed.

These experiments have been conducted for three regimes of vertical stratification: (i) Salt-finger favourable ('hot and salty' above); (ii) Diffusive convection favourable ('hot and salty' below); (iii) Doubly stable ('cold and salty' below).

One of our main conclusions concerns the driving mechanism for the horizontal intrusive flow. Away from the front or 'nose' of the intrusions, the lateral flows are no longer tilted but are horizontal. Here, finger layers alternate in the vertical with convecting layers. In these convecting layers, vertical transport of horizontal momentum by the Reynolds stress plays a major role in maintaining the lateral motion against viscous dissipation.

1. Introduction

This is a report on laboratory experiments on double-diffusive interleaving. These flows occur in fluids whose density is determined by two components, such as temperature (T) and salinity (S), which have different diffusivities. They result from an instability when there are horizontal gradients in T and S, with the simplest case being one in which the horizontal density gradient due to T is compensated by an opposing horizontal density gradient due to S, so that there are no net horizontal density gradients and therefore no density currents. However, an initial displacement of a parcel of fluid with property T, S along an isopycnal to an environment with a different combination of T and S could result in diffusion of T before any substantial diffusion of S, thus leading to density-driven flow. This instability has certain vertical wavelengths with associated multiple reversals in the flow.

Interleaving observed in the oceans has been attributed to a similar double-diffusive origin. Here, observations indicate multiple reversals in T with depth. These are

https://doi.org/10.1017/S002211200600992X Published online by Cambridge University Press

compensated by a similar structure of multiple reversals in S with depth, so that the density is often a monotonic function of depth. (See Ruddick & Richards 2003 for a review.) Their horizontal structure is coherent for many kilometres. Such structures have been observed in almost every ocean basin, but particularly at the confluence of two water masses, such as the Brazil Current–Malvinas Current confluence, or the Gulf Stream front. No doubt some of these are complicated by the fact that there is a baroclinic shear associated with the currents. However, if we considered an idealized case of water mass of property T_1, S_1 and density ρ_1 flowing adjacent to another water mass of property T_2, S_2, ρ_2 but with $\rho_1 = \rho_2$, heat exchange between the two could not occur by baroclinic instability. In this case, a double diffusive interleaving might be the only effective way to transfer heat and salt between these water masses. As these water masses then flow to other latitudes, it may be important to determine the magnitudes of this lateral heat and salt transfer and its result on global transport.

Many of the early studies of interleaving instability (Stern 1967; Turner & Chen 1974; Ruddick & Turner 1979; Ruddick, Phillips & Turner 1999) considered the case of a salt-fingering layer of fluid. Lateral displacements in this would lead to an enhanced salt-fingering below the intrusion and a subdued salt fingering above, for intrusive flows away from hot salty regions. It is this vertical divergence of the salt flux that leads to an intruding nose that rises as it moves away from the hot salty region.

The stability diagram for vertical forcing only can be seen in, for example, Turner (1973) figure 8.2. Here, positive salt Rayleigh number R_S means salting from below, while positive thermal Rayleigh number R_T means heating from below. Salt fingers occur in the third quadrant between $R_\rho = 1$ and $R_\rho = 1/\tau = 3$ for the present sugar–salt experiments. 'Diffusive convection' occurs in the first quadrant for $R_\rho > (\mathrm{Pr} + \tau)/(\mathrm{Pr} + 1) \approx 1$ for the present experiments. Here

$$R_\rho = R_T/R_S$$

$$R_T = \frac{g\alpha\Delta T}{\kappa_T \upsilon} d^3, \quad R_S = \frac{g\beta\Delta S}{\kappa_T \upsilon} d^3, \quad Pr = \frac{\upsilon}{\kappa_T}, \quad \tau = \frac{\kappa_S}{\kappa_T}$$

where g is the acceleration due to gravity, α the thermal expansion coefficient, β the salt contraction coefficient, κ_T the thermal diffusivity, κ_S the salt diffusivity, υ the kinematic viscosity and d the fluid-layer depth. For salt in water $\kappa_T = 10^{-5}\,\mathrm{cm^2\,s^{-1}}$, for sugar in water $\kappa_S = 3 \times 10^{-6}\,\mathrm{cm^2\,s^{-1}}$, $\upsilon = 10^{-2}\,\mathrm{cm^2\,s^{-1}}$, $Pr = 10^3$.

However, when horizontal gradients of T and S are superposed on vertical gradients, it may be helpful to refer to the following three cases: figures 1 shows isotherms, isohalines, and isopycnals for the three cases of doubly stable (figure 1*a*), diffusive favourable (figure 1*b*), and salt-finger favourable (figure 1*c*). Here 'doubly stable' refers to vertical stratification in the fourth quadrant, 'finger favourable' refers to vertical stratification in the third quadrant (even though R_ρ may exceed $1/\tau$ so that fingers would be stable for vertical forcing only), and 'diffusive favourable' refers to stratification in the first quadrant (even for $R_\rho < 1$ where diffusive convection may be stable for vertical forcing only). By moving parcels horizontally along an isopycnal to the left (towards colder fresher water) in the finger favourable figure 1(*c*), it is apparent that a small lateral displacement, without diffusion, leads to enhanced fingers below, subdued fingers above the intrusion. A larger lateral displacement leads to greater enhancement of fingers below and diffusive convection above the intrusion.

Similarly, displacing parcels to the left in the diffusive favourable figure 1(*b*), without diffusion, leads to greater diffusive convection above. A larger displacement to the left leads to greater diffusive convection above and salt fingering below.

https://doi.org/10.1017/S002211200600992X Published online by Cambridge University Press

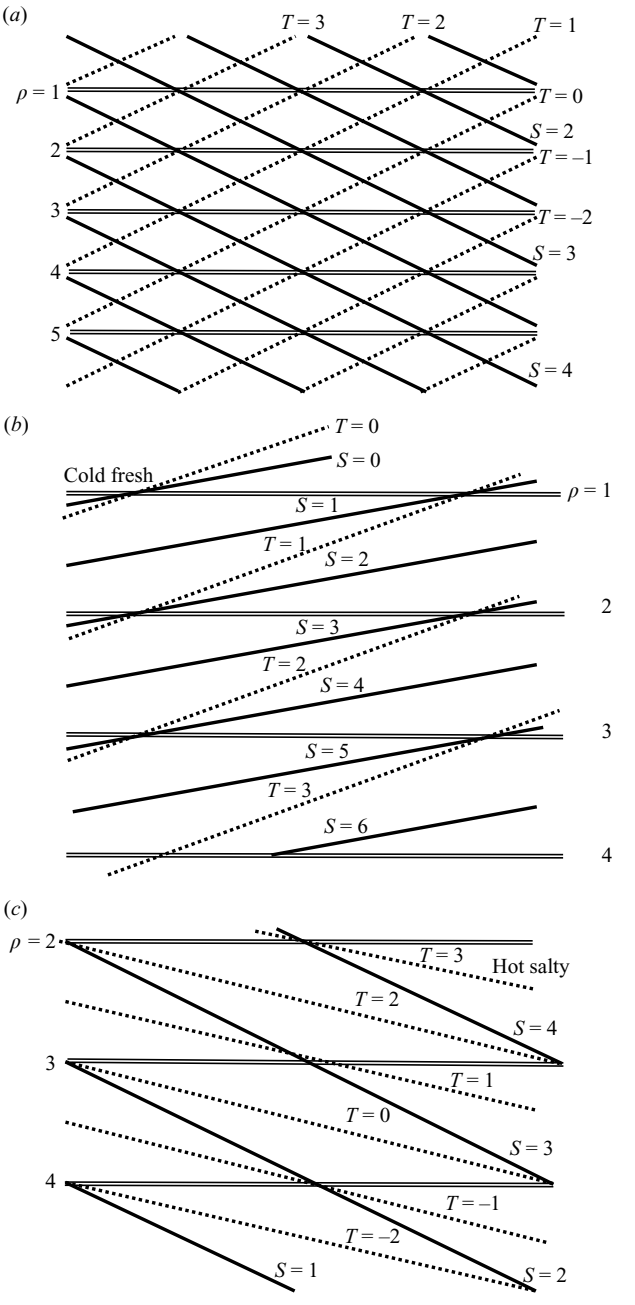


FIGURE 1. Isotherms, isohalines, and isopycnals for $\rho = 1 - T + S$, for the cases of (*a*) doubly stable, (*b*) diffusive favourable and (*c*) finger favourable stratification.

Finally, in the doubly stable case of figure 1(*a*), displacement sufficiently far to the left, without diffusion, leads to fingers above, diffusive convection below the intrusion, while displacement far enough to the right leads to diffusive convection above and finger instability below the intrusion.

For all of the cases above, if diffusion of the faster diffuser T is allowed, then lateral displacement leads to convective instability in each case.

https://doi.org/10.1017/S002211200600992X Published online by Cambridge University Press

While the salt-finger flux divergence is a most compelling argument for intrusions to slope upwards away from the hot salty regions, Holyer (1983) argues that fingers and diffusive convection are secondary instabilities that grow on the initial intrusive instability. She shows that lateral intrusions are unstable at zero horizontal Rayleigh numbers, that intrusions slope upwards towards the hot salty region since cold fresh parcels are warmed by the faster-diffusing heat.

In the classical experiments of Ruddick & Turner (1979), sugar (S) stratified fluid is separated from a salt (T) stratified fluid by a removable barrier. There is no horizontal gradient of either T or S, but a discontinuity at the barrier. When the barrier is removed, diffusion would make horizontal gradients. However, before the diffusion would have acted across one mm, intrusive flows have travelled tens of cm. These intrusions slope upwards to the sugar side in accordance with the vertical divergence of the 'salt' flux argument.

In the experiments reported here, continuous horizontal gradients of T were made to compensate the opposing continuous horizontal gradients of S. The arrangement is closer to the basic state of Holyer's theory. Yet lateral displacements have the immediate consequence of fingers and diffusive convection; this cannot be avoided. Furthermore the observed lateral flows had virtually no slope. The intrusive flows are horizontal except for initial transients or in the special case when intrusions entered a region of no horizontal gradient. It will be shown from particle image velocimetry (PIV) in this report that the convective layers of the intrusion have a Reynolds stress which transports horizontal momentum vertically, thereby helping to maintain a lateral shear flow against viscous disspiation.

2. Apparatus

As already implied, the faster diffuser in the ocean is temperature T; the slower diffuser is salinity S. In the laboratory we use salt for the ocean's cold and the slower diffusing sugar for the ocean's salt. This avoids the problems of uncontrolled heat exchange with the laboratory surroundings. Most of the continuous-gradient interleaving experiments reported here were performed in a small tank 24 cm deep (z-direction), 57 cm wide (x-direction) by 3.1 cm (y-direction). Experiments performed in the larger tank – 30 cm deep, 183 cm wide (x-direction) by 10 cm (y-direction) – with removable barrier and discontinuous properties across the barrier will be reported separately, but some reference to understanding gained from those experiments might be unavoidable.

The small tank was constructed to allow filling with fluid that would have horizontal gradients in T (salt), density-compensated by opposing horizontal gradients in S (sugar). Thus if the salt concentration increases with increasing x, the sugar concentration should decrease with increasing x in such a way that

$$\alpha \frac{\partial T}{\partial x} = \beta \frac{\partial S}{\partial x}$$

and there will be no horizontal density gradient.

The scheme that finally evolved was one in which fluid with the appropriate $T(x)$, $S(x)$ at a given z was introduced at each (discretized) location in x at the same flow rate as at every other location in x, this to avoid larger in-flow at one x flooding the neighbouring regions and producing erroneous gradients. The tank had 22 inlet tubes equally spaced along the bottom, attached to 22 syringes, each holding 5 ml of the appropriate solution. The 22 syringes can be plunged at the same rate by turning

https://doi.org/10.1017/S002211200600992X Published online by Cambridge University Press

two nuts on two vertical threaded rods, thus slowly lowering a horizontal bar on the syringes. This assures that the correct volume (as well as the correct $T(x)$, $S(x)$) is delivered at the same rate to each x.

Further apparatus included a 4 million pixel digital camera for PIV, a professional camera using 70 mm film for particle tracking velocimetry (PTV), a small 25 mw green laser, and a 2 w zirconium arc lamp with 1 mm diameter arc for the making of shadowgraphs. A specific gravity balance accurate to the fourth decimal place was also used. The experiments were conducted in a dark room for photographic purposes.

3. Procedure

3.1. *Preparing the fluid and filling the tank*

As in Holyer's stability analysis we wish to produce a density profile

$$\rho(x, z) = \rho_0[1 - \alpha T(x, z) + \beta S(x, z)],$$

with

$$\alpha T(x, z) = ax + bz, \tag{1a}$$

$$\beta S(x, z) = ax + cz, \tag{1b}$$

since then, $\alpha \partial T/\partial x = \beta \partial S/\partial x$.

The vertical density gradient is $-b + c$ and its lower limit is chosen for ease in assembly; the smaller the vertical density gradient, the more care is required to prevent accidental overturning while filling the tank. The vertical density ratio R_ρ^v, defined as

$$R_\rho^v = \frac{\alpha \partial T/\partial z}{\beta \partial S/\partial z}$$

is here equal to b/c and is one of the main control parameters. By choice of the magnitude and sign of b and c, we can conduct experiments in 'salt-finger favourable' or 'diffusive favourable' or 'doubly stable' conditions. The horizontal density ratio, defined as

$$R_\rho^h = \frac{\alpha \partial T/\partial x}{\beta \partial S/\partial x}$$

is always equal to unity in these experiments.

An approximation to the fields in equation (1) may be produced by considering the fluid as discretized into bins, with each bin labelled for its location in x, z by indices i, j. Fluid for each bin is made with the appropriate T and S concentration. To make these fluids for each bin, we proceeded as follows: four barrels of solution, labelled TL, BL, TR and BR (for top left, bottom left, top right and bottom right, respectively) were produced using sugar SU (for S) and salt SA (for T), dissolved in 'treated' distilled water. The treatment is the addition of a small quantity of sodium fluoride to prevent microbial growth, plus the addition of a fine powder of 10 μm sized beads for the purpose of PIV. An example is given in table 1.

Next the fluid from the barrels TL and BL was partitioned into 11 buckets as follows: the top bucket (1L) contains 10 parts by volume of TL fluid, zero parts of BL fluid; the next bucket (2L) contains 9 parts of TL and 1 part of BL; and so on, until the bottom bucket (11L) contains zero parts TL and 10 parts BL. A similar procedure with barrels TR and BR produced 11 buckets, 1R (containing 10 parts

https://doi.org/10.1017/S002211200600992X Published online by Cambridge University Press

TL	TR
53.3 g SA	0 g SA
21.0 g SU	123.4 g SU
1.0 l H_2O	1.0 l H_2O
$\rho = 1.0214$	$\rho = 1.0214$
BL	BR
163.0 g SA	106.6 g SA
0 g SU	100.0 g SU
1.0 l H_2O	1.0 l H_2O
$\rho = 1.0801$	$\rho = 1.0801$

TABLE 1. Composition of fluids.

TR, zero parts BR) through 11R (containing zero parts TR, 10 parts BR). In some earlier experiments we used 18 instead of 11 buckets, thus making 18 layers.

The top buckets 1L and 1R were partitioned into 22 cups, ranging from 10 parts of 1L and zero parts of 1R in the leftmost cup, to 0.45 parts of 1L and 9.55 parts of 1R in the rightmost cup. Thus 22 cups were filled for the top level (level 1) of the fluid to be placed in the tank; these are cups $j = 1$, $i = 1$ to 22. A similar procedure of partitioning buckets 2L and 2R was used to produce cups $j = 2$, $i = 1$ to 22, and so on until $j = 1$ to 11, $i = 1$ to 22 were all filled, for a total of 242 cups.

From each cup, 5.0 ml were sucked into each of 242 syringes held ready in an 11×22 grid. The tank to contain the working fluid was filled one layer at a time (starting with $j = 1$), using the 22 syringes $j = 1$, $i = 1$ to 22, of course maintaining their order from left to right. Each syringe is connected to a length of (all equal) 1 mm diameter tubing which leads to 22 identical openings 1 mm in diameter. These openings are equally spaced (2.54 cm apart) along the bottom of the tank. Thus each 5 ml volume of fluid in each syringe fills a volume in the tank 2.54 cm by 3.1 cm by 0.63 cm in height. To fill the layer $j = 1$, the 22 syringes are arranged on a holder and all 22 are slowly plunged at the same rate so that fluid from each fills its designated part of the tank; no one should flow faster than others, for this would flood over into undesignated parts of the tank.

To fill the next layer, $j = 2$, the syringe holder is raised 0.63 cm to prevent backflow when the 22 syringes for $j = 1$ are removed and replaced with those for $j = 2$. These 22 syringes are then slowly plunged at the same rate, and so on until all 11 levels are filled. This procedure takes approximately 2 h.

Finally, several experiments were run with horizontal gradient only in the middle third of the tank (the middle 8 syringes) while the left-hand third (the left-hand 7 syringes) was stratified only with sugar, and the right-hand third (the right-hand 7 syringes) was stratified only with salt. These will be labelled the 'middle third experiments'.

3.2. *The shadowgraphs*

The syringe holder was released after filling the tank and laid horizontal to avoid obstructing the view through the working fluid. In the dark, unexposed photographic paper 25 cm high and approximately 1 m in length was placed on a target surface which was usually 60 cm behind the tank. Light from a 'point' source (the zirconium arc lamp, with arc diameter 1 mm) was placed usually 60 cm before the tank. At these

https://doi.org/10.1017/S002211200600992X Published online by Cambridge University Press

distances, exposure times were usually 10 to 15 s. The exposed paper was then placed in a light-tight box for later development.

3.3. *PIV and PTV*

For this application, a sheet of laser light illuminated a vertical (x, z)- plane, mid-distance in y. A 4 million pixel digital camera, usually 30 cm from the illuminated fluid, was used to photograph the 10 μm particles in an area 10 cm in x by 7.5 cm in z, at set intervals in time. This time interval was chosen to resolve horizontal intrusive flows, but the same interval would not resolve the slow flow in the fingers. The program PIV Sleuth was used to obtain flow vector fields from the displacements of these particles.

For PTV (particle tracking velocimetry), the same illumination and optical arrangement was used, but data were obtained by multiply exposing 70 mm photographic film according to certain protocols. One such protocol (the 'slow protocol') was 30 s on, 60 s off, repeated 5 times in succession; the sixth time was 30 s off, 60 s off, then 30 s on, 60 s off; repeated 3 times, where 'on' means the laser light is on. This would produce on the film a line of 5 bright dots followed by one dark or blank spot, followed by 3 bright dots. The distance between the bright dots, divided by the time 90 s gives the particle speed, and its direction is deduced from the asymetrical placement of the blank spot. For faster flows, the following protocol (the 'fast protocol') was used: 10 s on, 20 s off; repeated 5 times, followed by 10 s off, 20 s off, followed by 10 s on, 20 s off repeated 3 times. The PTV data was not used to obtain vector flow fields, but as a complement to the shadowgraphs in places where there was fast flow but little refractive index variation.

4. Observations

The shadowgraphs show the general structure of the interleaving. Those shown in figures 2 to 4 are excerpts showing 30 cm width out of the total of 110 or 120 cm photograph width. The 30 cm segment shown is indistinguishable from any other 30 cm segment that could be extracted from the full photograph. The magnification can be deduced from the scale shown on the photograph.

All the shadowgraphs show horizontal banded structures, with alternating layers of salt fingers and convection. The exception was in initial transients as shown at the bottom of the figure 2(*a*)(i) where the latest-formed layer shows tilted interleaving. These tilted structures last only 10–20 min after the introduction of the fluid into the tank is completed. In the salt-finger-favourable cases, salt fingers dominate the image, but convecting layers are always present between the finger layers. In the diffusive-favourable cases, convective plumes are evident in shadowgraphs soon after creation of the stratified fluid, but after some time (of the order of hours) this convective layer is often a blur. The PIV will show that these convective regions have strong lateral shearing flows.

Among the finger-favourable cases shown, a progression is evident as R_ρ^v is decreasing from 10 in figure 2(*a*)(i) to $R_\rho^v = 4$ in figure 2(*a*)(ii) to $R_\rho^v = 2$ in figure 2(*a*)(iii). The relative depths of the finger zone d_f to the convection zone d_c are approximately as shown in table 2.

Figures 2(*b*)(i) and 2(*b*)(ii) at $R_\rho^v = 10$ were chosen to show the relative magnitudes of velocity in the finger zone and in the convection zone. In the figure 2(*b*)(i), the region enclosed in the black box shows a thin convecting layer on top, with tilted convecting plumes; below this is a relatively deeper layer of fingers in a roughly S

https://doi.org/10.1017/S002211200600992X Published online by Cambridge University Press

R_ρ^v	d_f	d_c
10	0.60	0.40
4	0.75	0.25
2	0.90	0.10

TABLE 2. The relative depths of the finger zone d_f to the convection zone d_c.

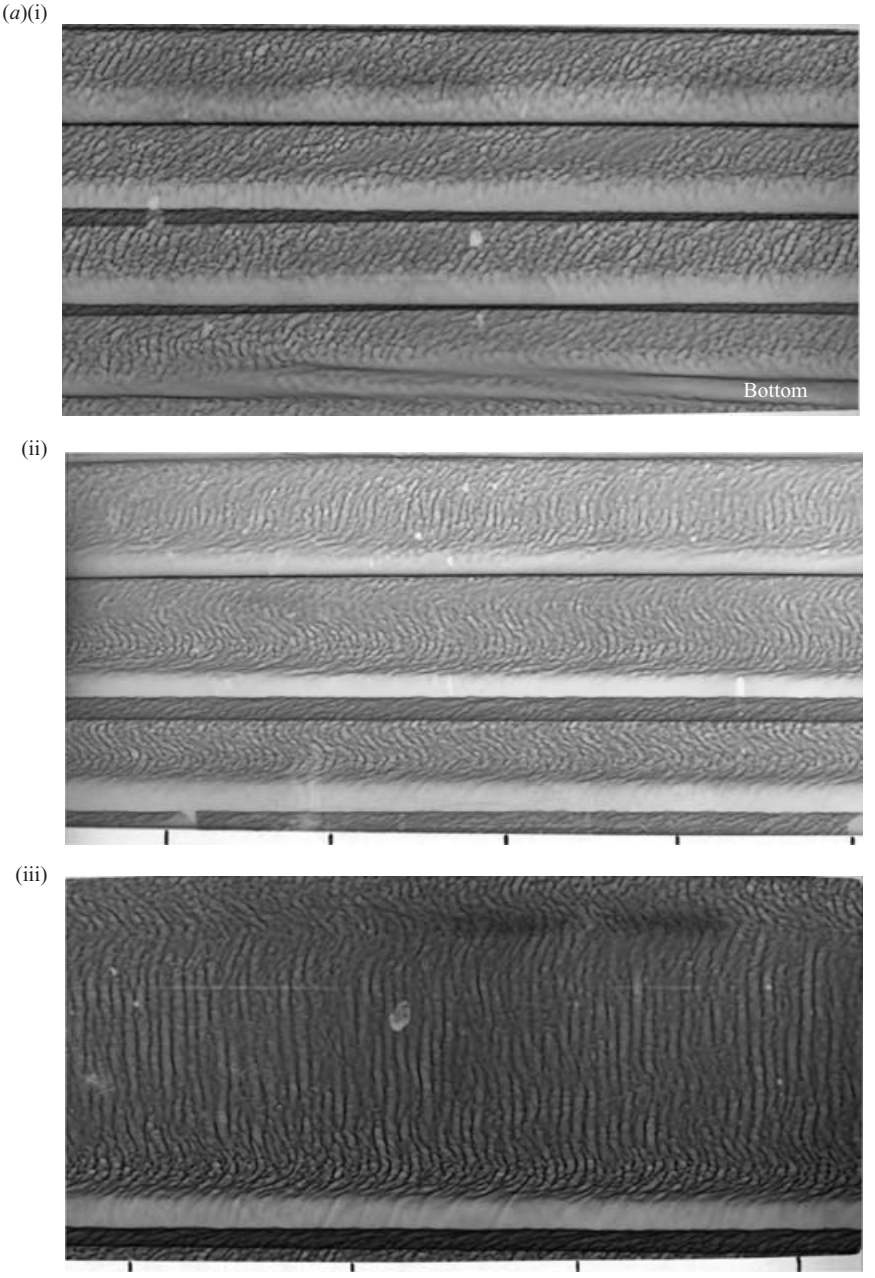


FIGURE 2(*a*). For caption see facing page.

https://doi.org/10.1017/S002211200600992X Published online by Cambridge University Press

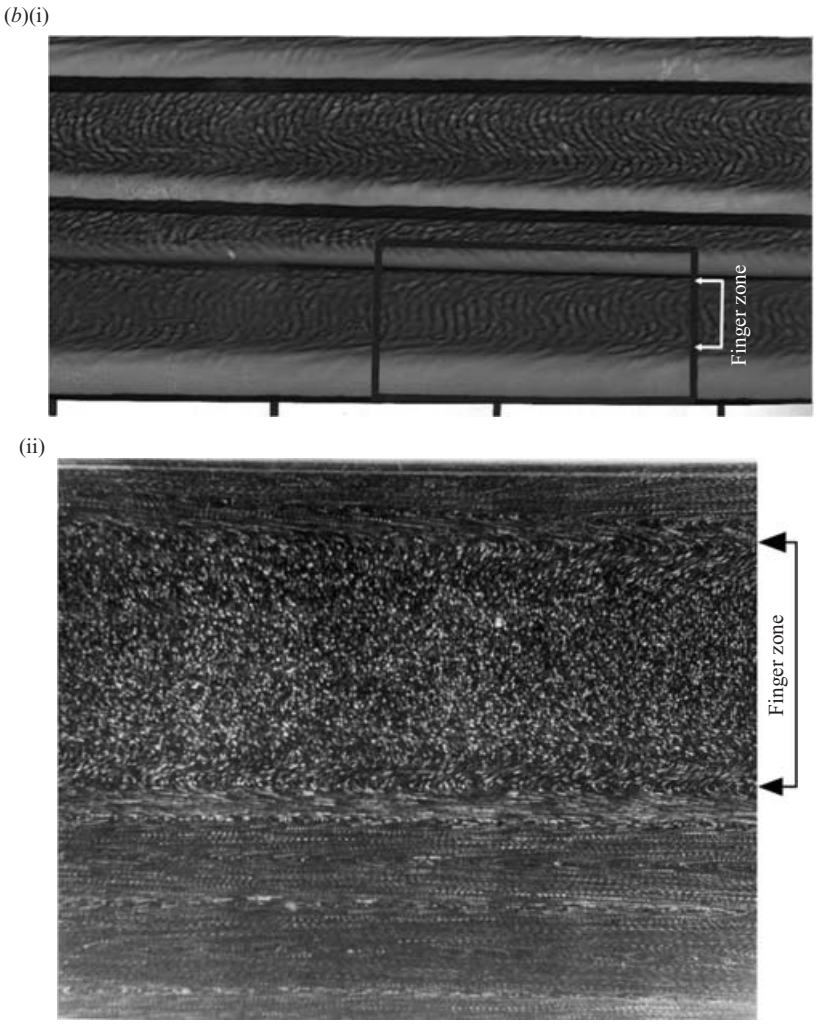


FIGURE 2. (*a*) Shadowgraphs showing salt-finger favourable interleaving. The long edge of the photograph is in the direction of the horizontal x-axis. The tick marks along the horizontal are 2.54 cm apart. (i) $R_\rho^v = 10$; (ii) $R_\rho^v = 4$; (iii) $R_\rho^v = 2$. (*b*) (i) Shadowgraph of salt finger favourable interleaving at $R_\rho = 10$. Fingers show prominently, but the convection zone is a uniform white blur. The black box is the region of the PTV in (*b*) (ii). (ii) PTV of the region of the black box in (*b*) (i) shows fast shearing flows in the convection zone, and almost undetectable flow in the finger zone. Time between dots is 30 s (see text for protocol).

shape, then below this is a convecting layer which is blurred. Figure 2(*b*)(ii) shows a PTV image of the boxed area. The fast protocol was used.

First, it is noted that speeds in the convection zone are at least an order of magnitude larger than in the finger zone. Much of the finger zone appears to be motionless on this time scale. Secondly, there are reversals in flow direction in the convection zone. Wedge-shaped patterns identifiable in the convection zone might look like intrusions, but actually the velocity on the top of a leftward-pointing wedge is rightwards while the velocity on the bottom of the same leftward pointing wedge is leftward. The particle tracks also have a vertical component to their velocity, so that

https://doi.org/10.1017/S002211200600992X Published online by Cambridge University Press

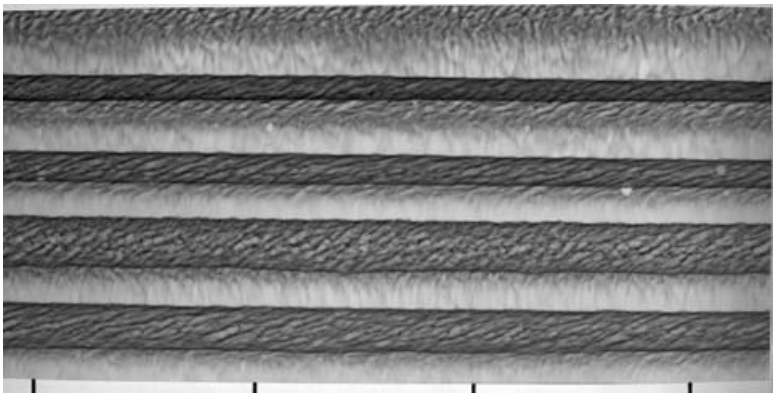


FIGURE 3. Shadowgraph of diffusive convection favourable interleaving at $R_\rho^v = \frac{1}{2}$.

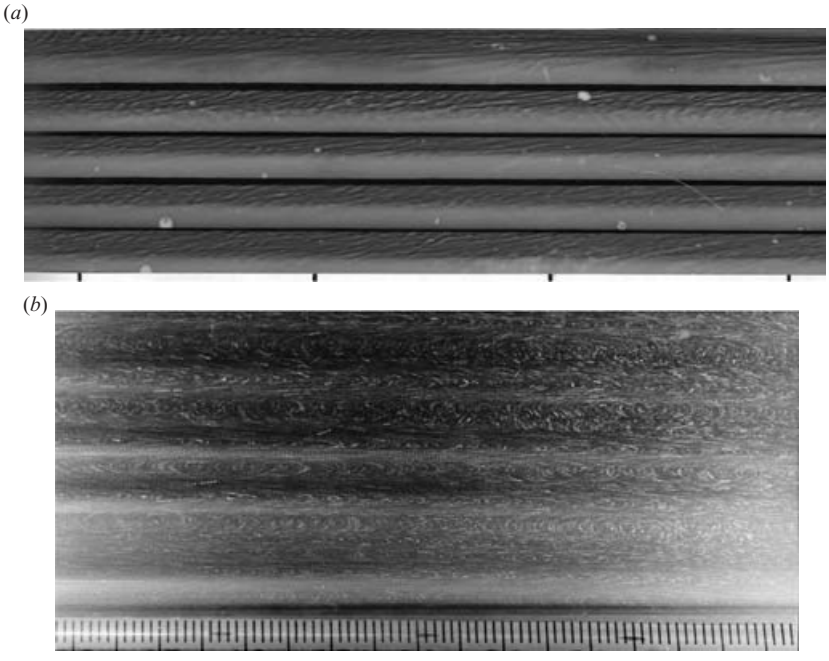


FIGURE 4. (*a*) Shadowgraph of doubly stable interleaving. (*b*) PTV of doubly stable interleaving. The time between dots is 30 s (see text for protocol). The scale is in mm.

Reynolds stresses $\overline{uw}$ may be important. However, in the finger zone such stresses will be orders of magnitude smaller.

Figure 3 shows a portion of a shadowgraph excerpted as in figure 2(*a*), but for the diffusive-favourable case. It is at $R_\rho^v = 0.5$ and shows prominent horizontal bands of convective plumes alternating with finger layers.

Similarly, figure 4(*a*) shows a shadowgraph of a doubly stable case of lateral intrusions. Again the layers are horizontal, and the finger zone and convection zone appear to occupy nearly equal heights. The finger activity appears to be subdued compared to those in the finger-favourable cases in figure 2(*a*).

https://doi.org/10.1017/S002211200600992X Published online by Cambridge University Press

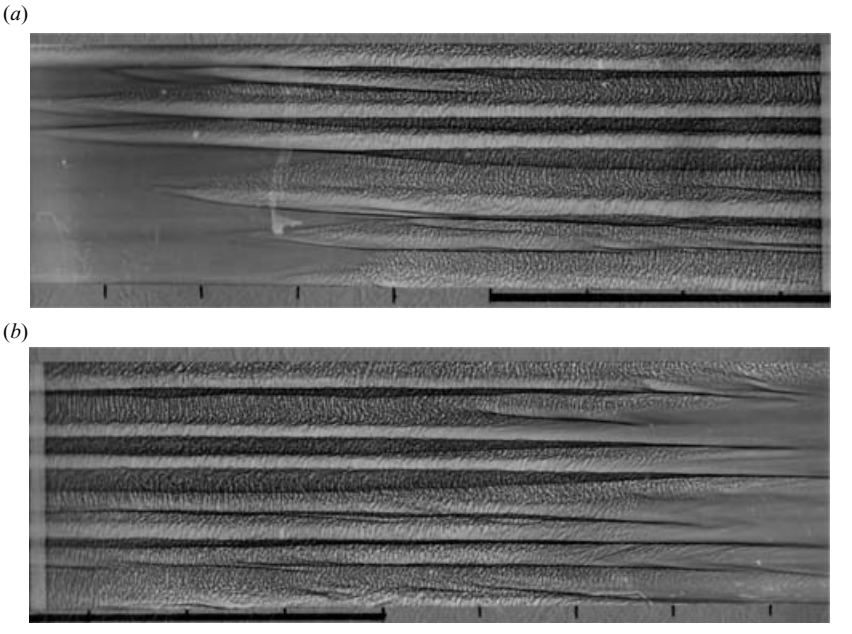


FIGURE 5. Shadowgraph showing interleaving on a continuous gradient, intruding into regions of no horizontal gradient. The distance between lines on the scale is 2.54 cm. The heavy black line along the bottom indicates the 'middle third' where continuous property gradients were initially imposed. The shadowgraph is shown in two parts because of limitations of the scanner. The vertical band at mid-distance is a shadow of a mark on the tank wall.

Figure 4(*b*) shows a PTV image of the doubly stable intrusive flow. It shows horizontal banded structures with bands of nearly circular or elliptical flow lines; these are separated in the vertical by bands of more nearly linear flow lines which have the appearance of forming a wedge. As in the convection zone of the finger-favourable case, the flow is in opposite directions above and below these wedges. Also as in the finger-favourable case, these wedge flows have sloping trajectories so that the Reynolds stress $\overline{uw}$ may be important in the maintenance of the mean flow.

Finally, figures 5(*a*) and 5(*b*) show the left- and right-hand portions of one shadowgraph of the 'middle third' experiment. The part with the initially imposed horizontal gradient is shown with a heavy black bar along the bottom of the shadowgraph, $R_\rho^v = 10$. (The greyish vertical bar is just a shadow of a mark on the wall at mid-distance in x. The fluid is continuous through this point.) The intrusions into the laterally unstratified regions are reminiscent of the shadowgraphs of Ruddick & Turner (1979) where a gate was lifted which was separating sugar (only) stratified fluid from salt (only) stratified fluid. Here, however, both the finger zones and the convection zones are clearly seen.

Figure 6 shows the velocity fields derived from PIV. These are typical of the many plots obtained. Figure 6(*a*) is for a finger favourable case, figure 6(*b*) for a diffusive favourable case and figure 6(*c*) for a doubly stable case. Panels (i) of figure 7 show $\bar{u}$ the horizontal averaged u, averaged over the 10 cm horizontal extent of the PIV photograph. Panels (ii) show the corresponding Reynolds stress $\overline{uw}$ as it varies with z. The irregularity in z of $\overline{uw}$ may be attributable to the observation that in the 10 cm width there are only a few (less than 10) tilted swirling flows which must be

https://doi.org/10.1017/S002211200600992X Published online by Cambridge University Press

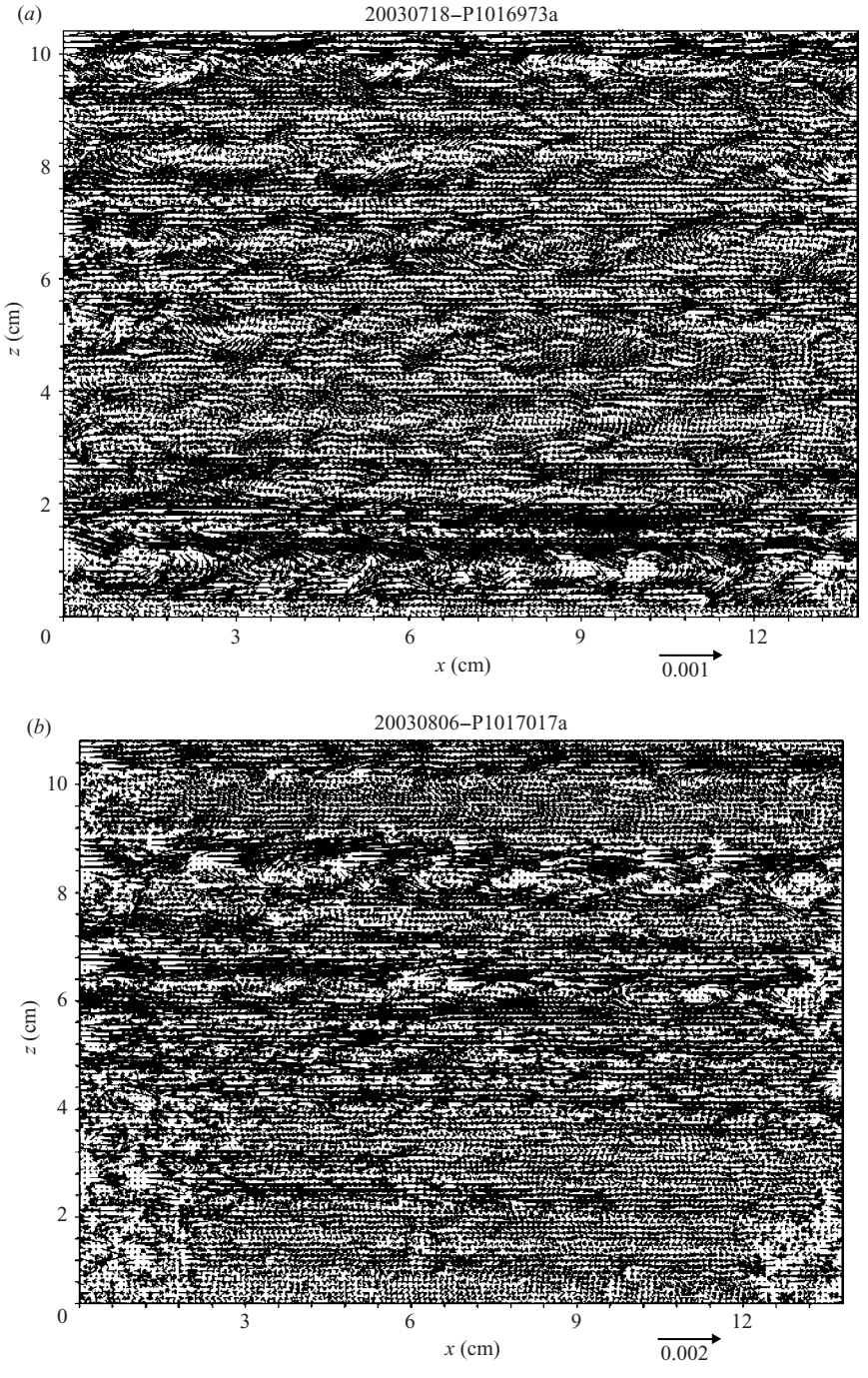


FIGURE 6(*a*, *b*). For caption see facing page.

contributing to the horizontal average stress. Panels (iii) and (iv) show $\bar{u}$ and $\overline{uw}$ for a portion of the same velocity field. The portions (usually a half or a quarter of the whole) selected showed a clear relation between $\bar{u}$ and $\overline{uw}$. From these right-hand

https://doi.org/10.1017/S002211200600992X Published online by Cambridge University Press

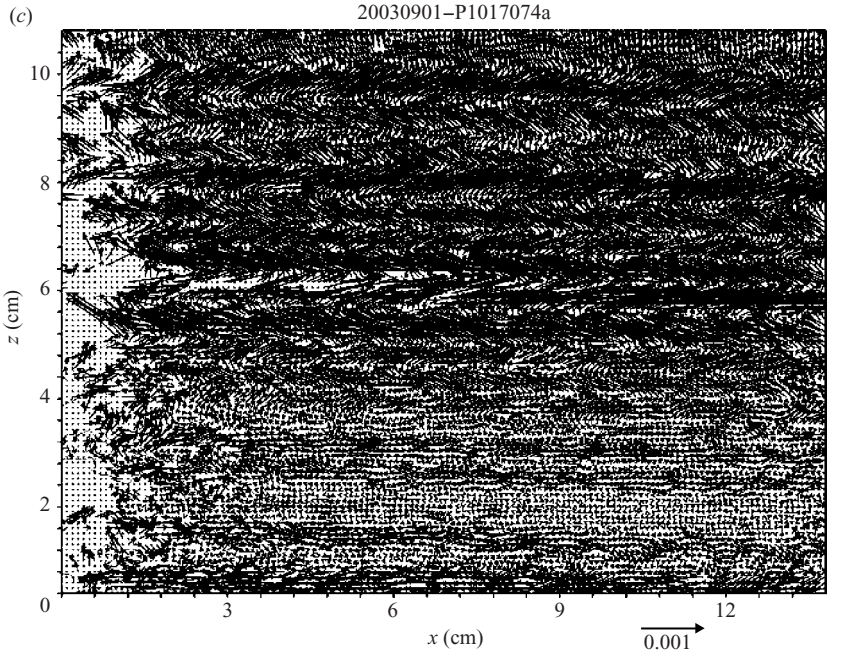


FIGURE 6. Velocity field derived from PIV. The domain photographed was 13 cm in x, 10 cm in z. The magnitude shown with the arrow is in mm m^{-1} s^{-1}. (*a*) Finger favourable. (*b*) Diffusive convection favourable. (*c*) Doubly stable.

Frame number \ Peak number	1	2	3	4	5	6
20030718-P1016973a (finger favourable)	0.87	0.37	0.50			
20030806-P1017017a (diffusive favourable)	0.16	0.38	1.0	0.67	0.54	
20030901-P1017017a (doubly stable)	0.63	0.88	1.0	1.0	1.5	1.0

TABLE 3. Ratios of momentum flux by the Reynolds stress to that by the viscous stress, $\overline{uw}/\nu\Delta\bar{u}/\Delta z$

panels, $\nu\Delta\bar{u}/\Delta z$ and $\overline{uw}$ were computed and their ratios shown in table 3. The three cases shown are as for figure 6.

The main result is that the magnitude and sign of the Reynolds stress are such as to help maintain the mean flow $\bar{u}$ against viscous dissipation in certain parts of the flow field. The basis for this observation is the following: if a horizontally unbounded fluid has horizontal velocity component u which is separated into horizontal mean part $\bar{u}$ and fluctuating part u', and vertical velocity w likewise into w' and $\bar{w}$, the horizontally averaged momentum equation is

$$\frac{\partial\bar{u}}{\partial t}+\frac{\partial}{\partial z}\overline{u'w'}=\nu\frac{\partial^2\bar{u}}{\partial z^2}, \tag{2}$$

where ν is the kinematic viscosity (here $\nu=10^{-2}$ cm^2 s^{-1}). For steady $\bar{u}$, the first integral of (2) is

$$\overline{u'w'}-\nu\frac{\partial\bar{u}}{\partial z}=M, \tag{3}$$

https://doi.org/10.1017/S002211200600992X Published online by Cambridge University Press

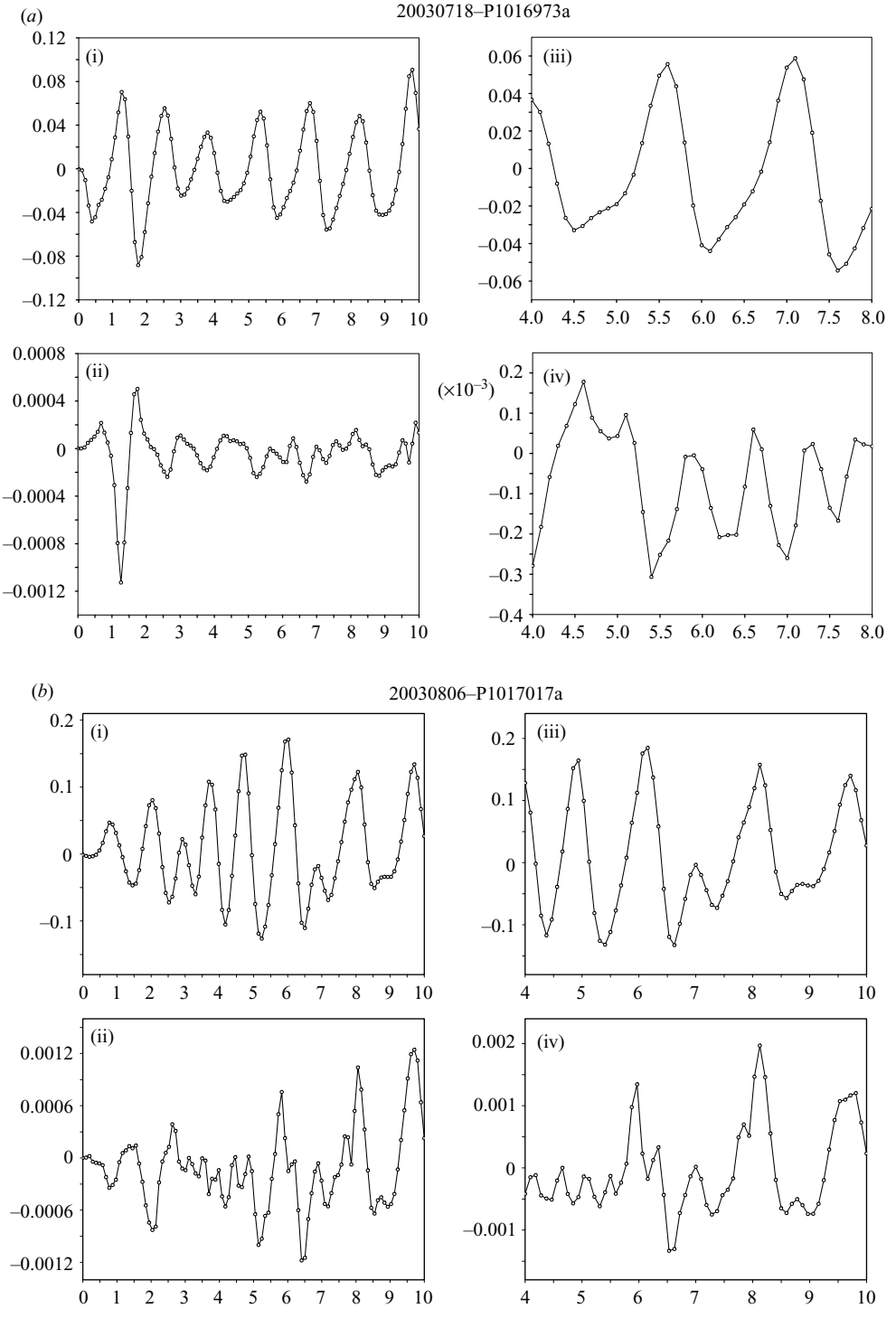


FIGURE 7(*a*, *b*). For caption see facing page.

https://doi.org/10.1017/S002211200600992X Published online by Cambridge University Press

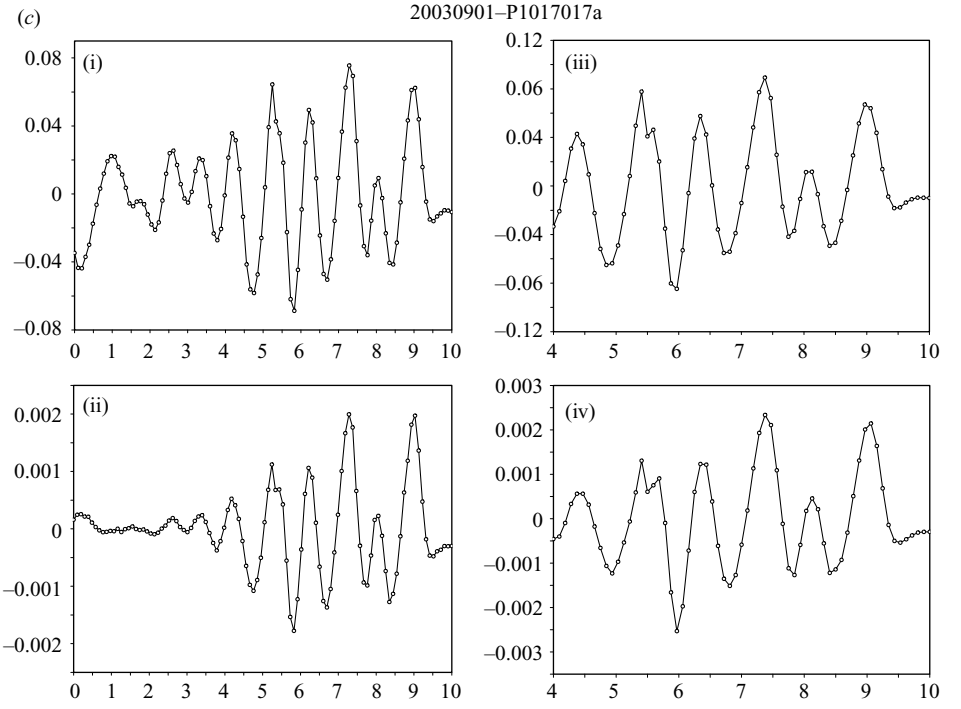


FIGURE 7. Horizontal averages over the domain (13 cm in x) of the horizontal velocity $\bar{u}$ (cm s^{-1}) and of the Reynolds stress $\overline{uw}$ (cm^2 s^{-2}) as they vary with vertical coordinate z (cm). The two right-hand panels are for smaller portions of the whole field (see text). (*a*) Finger favourable. (*b*) Diffusive convection favourable. (*c*) Doubly stable.

where M is a constant independent of z. For example if $M = 0$, the Reynolds stress must be opposite in sign to that of the viscous momentum flux. The latter is always down-gradient; the Reynolds stress would then transport horizontal momentum vertically, up the mean gradient.

The kinetic energy of the mean flow can be written as follows:

$$\frac{\partial}{\partial t}\left(\frac{\bar{u}^2}{2}\right)_m = \left(\overline{u'w'}\frac{\partial \bar{u}}{\partial z}\right)_m - \nu\left(\frac{\partial \bar{u}}{\partial z}\right)_m^2, \tag{4}$$

where the subscript m represents a volume average. Thus the kinetic energy of the mean flow $\bar{u}$ has a tendency to increase with time if the Reynolds stress $\overline{u'w'}$ and the mean shear $\partial\bar{u}/\partial z$ have the same sign. An example is shown in figure 8. The shading indicates regions where the stress and the shear have the same sign.

In addition to the sign of the stress and of the mean gradient, the magnitudes must be considered. In the convection zones, u', w' and $\bar{u}$ are of the same order of magnitude.

$$\bar{u} \sim 10^{-1} \text{ to } 10^{-2} \text{ cm s}^{-1},$$
$$\overline{u'w'} \sim 10^{-3} \text{ to } 10^{-4} \text{ cm}^2 \text{ s}^{-2},$$

For depths $\Delta z \sim 1$ cm,

$$\nu\frac{\Delta \bar{u}}{\Delta z} \sim 10^{-3} \text{ to } 10^{-4} \text{ cm}^2 \text{ s}^{-2}.$$

https://doi.org/10.1017/S002211200600992X Published online by Cambridge University Press

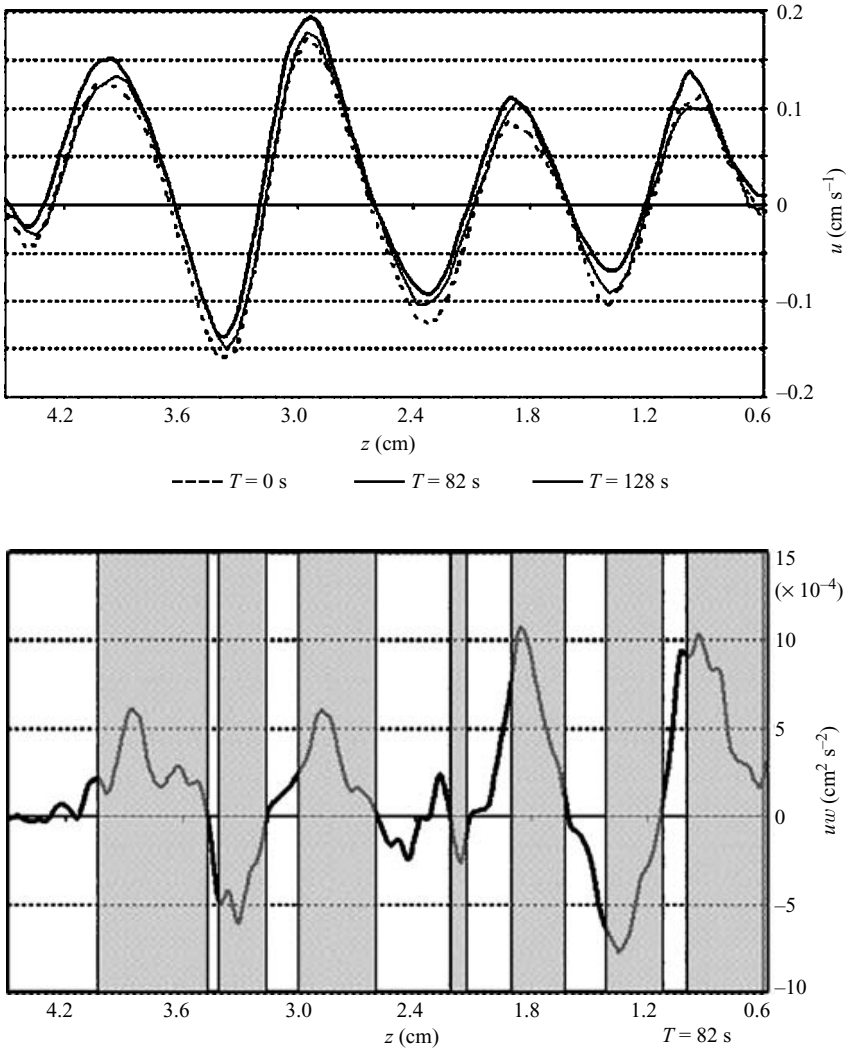


FIGURE 8. Mean flow $\bar{u}$, Reynolds stress $\overline{uw}$ for doubly stable case. The shading shows regions where $\partial\bar{u}/\partial z$ and $\overline{uw}$ have the same sign, and where the Reynolds stress term of equation (4) has a tendency to increase the kinetic energy of the mean flow.

Thus in the convection zone, the ratio of $\overline{u'w'}$ to $\nu\Delta\bar{u}/\Delta z$ is of order 0.1 to 1.0. Values of this ratio, obtained for the right-hand panels of figure 6(*b*), are shown in table 3. In the finger zone, however,

$$\bar{u} \sim 0 \text{ to } 10^{-3} \text{ cm s}^{-1},$$
$$u' \sim w' \sim 10^{-4} \text{ cm s}^{-1}.$$

Thus $\overline{u'w'} \sim 10^{-8}\,\text{cm}^2\,\text{s}^{-1}$ and does not contribute significantly to balance $\nu\Delta\bar{u}/\Delta z$ which is of order $10^{-5}\,\text{cm}^2\,\text{s}^{-1}$.

It would appear that fingers are tipping in the shear flow, but their momentum fluxes by the Reynolds stresses are orders of magnitude too small to contribute to the momentum balance. (See also figure 2(*b*)(ii) and related description.) In the

https://doi.org/10.1017/S002211200600992X Published online by Cambridge University Press

convection zone, however, the tilted convecting flows can contribute significantly to the maintenance of $\bar{u}$ against viscous dissipation.

The acceleration term $\partial\bar{u}/\partial t$ in equation (2) is an order of magnitude smaller than $\nu\partial^2\bar{u}/\partial z^2$. Thus, where the Reynolds stress term does not balance the viscous term, the residual must be due to a pressure gradient. The reason for the irregular nature of the data in table 4 is not understood.

5. Discussion

Although the continuous horizontal gradients of T and S resemble the basic state of Holyer's instability theory, tests of the theory, such as the predicted slopes of the interleaving layers, could not be made as lateral intrusions immediately produce the secondary instabilities of fingers and diffusive convection. Initial transient slopes in the finger favourable cases did slope up towards the 'hot salty' region as predicted by Holyer, but these slopes quickly disappeared and were replaced by horizontal layers. The Ruddick argument that these intrusions with enhanced finger flux of salt out of the layer would slope up towards the cold fresh region of a finger-favourable fluid was observed when intrusions entered a stable region with no horizontal gradient. Otherwise most of the interleaving flow was horizontal with alternating layers of fingers and diffusive convection, in all three categories: 'finger favourable', 'diffusive favourable', and 'doubly stable'.

The PIV results have shown that in the convection zone, the Reynolds stress divergence $\partial\overline{u'w'}/\partial z$ plays a major role in the momentum balance, being comparable (10% to 100%) to the viscous deceleration $\nu\partial^2\bar{u}/\partial z^2$. From the observed tilted convective plumes, it appears that there is up-gradient momentum flux maintaining the horizontal flow against viscous dissipation. The result of these observations especially as shown in figure 8, leads to the conceptual mechanism depicted in figure 9. Here we consider an initial disturbance $\tilde{U}(z,t)$ which consists of alternating leftwards and rightwards flow, and which we seek to amplify. We suppose that parcels of fluid advected by $\tilde{U}$ retain their initial salinity, but their temperatures equilibrate by diffusion to match their new surroundings. This leads to a convective overturning as shown in figure 9. These may develop a lower-left-to-upper-right tilt, or a lower-right-to-upper-left tilt (Howard & Krishnamurti 1986). However, in view of the pre-existing $\tilde{U}(z,t)$, it appears that the former might prevail. The vertical parts of the overturning would then transport rightward momentum upwards, from level $\rho=4$ to level $\rho=2$, and leftward momentum downwards, from level $\rho=2$ to level $\rho=4$. Thus such a convective flow would reinforce the initial $\tilde{U}(z,t)$, leading to a lateral intrusive instability.

6. Summary and conclusions

The initial vertical stratification was chosen in almost every case to be stable and in the following parameter ranges. For the finger-favourable cases we used $2\leqslant R_\rho^v\leqslant 10$ where $R_\rho^v<3$ would be necessary for salt-fingering instability. (The only vertically unstable case was for $R_\rho^v=2$.) For the diffusive-favourable cases we used $0\leqslant R_\rho^v\leqslant 1$ where $R_\rho^v>1$ is necessary for diffusive convection with only vertical forcing. For the doubly stable case, with $R_S^v>0$ and $R_T^v<0$, no vertically forced instability is possible. In each case the horizontal gradients of T and S were density-compensated so that the horizontal density ratio $R_\rho^h=1$. Theoretically the critical value of R_S^h and R_T^h is zero for the onset of lateral intrusions.

https://doi.org/10.1017/S002211200600992X Published online by Cambridge University Press

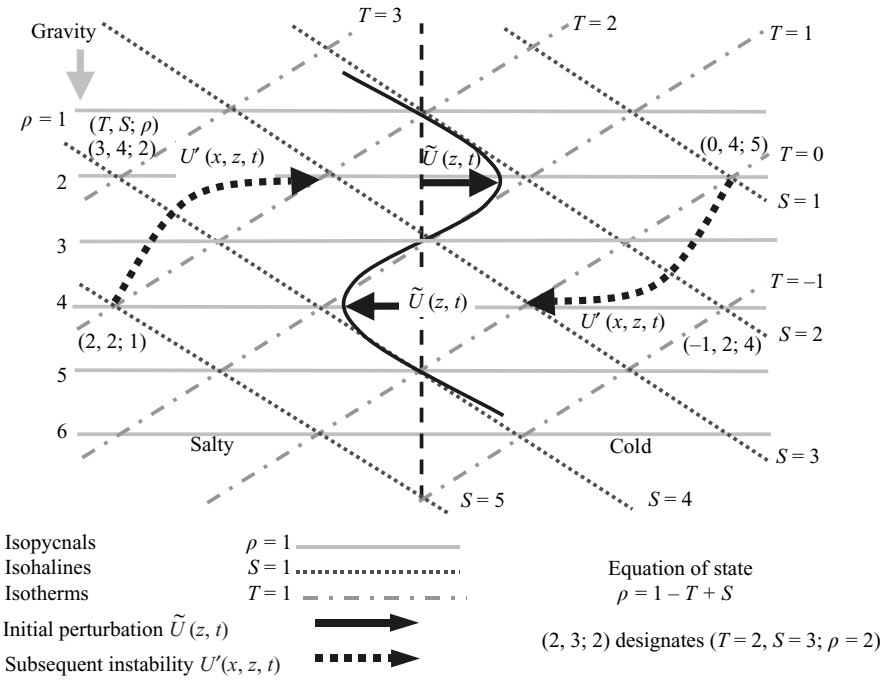


FIGURE 9. An instability mechanism for intrusion in doubly stable stratification. A parcel with initial property ($T=3$, $S=4$; $\rho=2$), advected to the right by the perturbation flow $\tilde{U}(z,t)$, enters progressively colder regions and itself becomes colder by heat diffusion while retaining its original high salinity, thus approaching ($T=0$, $S=4$; $\rho=5$). Likewise, a parcel with initial property ($T=-1$, $S=2$; $\rho=4$), advected to the left by perturbation flow $\tilde{U}(z,t)$, enters progressively warmer regions and itself becomes warmer by heat diffusion while retaining its original low salinity, and approaches ($T=2$, $S=2$; $\rho=1$). Convective overturning occurs because of the local unstable stratification. If this convective flow has a tilt from lower left to upper right, leading to a horizontal average Reynolds stress $u'w'$ positive on x-average, then rightwards momentum is transported up to where $\tilde{U}(z,t)$ is rightward, and leftwards momentum is transported down to levels where $\tilde{U}(z,t)$ is leftward, thereby reinforcing the initial perturbation velocity $\tilde{U}(z,t)$. Thus an instability can be expected to grow.

In all three cases, lateral intrusive flows occurred with salt-fingering below a 'hot salty' intrusion, and diffusive convection above it. The ratio of thickness of fingering layer to diffusive layer decreased systematically as R_ρ^v was increased from 2 to 10. Shadowgraphs showed tilted plumes in the convecting layer; these were more pronounced in the diffusive-favourable cases. In all three cases, this layer often appeared as a uniform blur in shadowgraphs, where the lateral shearing flows might be expected to decrease refractive index contrasts associated with plumes.

By comparing shadowgraphs, PTV and PIV, we concluded the following:

(i) The layered flows were horizontal. The only exceptions were in initial transients and in the case of a 'nose' intruding into regions with no horizontal gradients.

(ii) Salt fingers are very clear in shadowgraphs where they appear to be tilted by the lateral flows in adjacent layers, these being oppositely directed above and below the finger layer.

(iii) In PTV, the salt fingering layer shows orders of magnitude slower flows than in the convecting/lateral flow layer.

https://doi.org/10.1017/S002211200600992X Published online by Cambridge University Press

(iv) PIV results show that in the convecting/lateral flow layers, the vertical transport of horizontal momentum by the Reynolds stress $\overline{uw}$ was often comparable to the viscous transport $\nu \mathrm{d}\bar{u}/\mathrm{d}z$. Furthermore, the sign of $\overline{uw}$ and of $\mathrm{d}\bar{u}/\mathrm{d}z$ are such as to increase the kinetic energy of the $\bar{u}$ flow in parts of the fluid domain. Thus, in the convecting layer, the Reynolds stress may help maintain the lateral flow against viscous deceleration. This result does not hold for the fingering layer.

I wish to acknowledge many helpful discussions with Dr Robin Kung, especially concerning experiment design. I am also grateful to Professor Ron Adrian for providing us with the data analysis program PIV Sleuth, and to T. N. Krishnamurti and his staff for help with computing problems. This research was supported in part by the National Science Foundation under grant number OCE-0242535. This is contribution number 447 of the Geophysical Fluid Dynamics Institute at Florida State University.

REFERENCES

Christiansen, K., Soloff, S. M. & Adrian, R. J. 2001 PIV Sleuth: integrated particle image velocimetry (PIV) interrogation/validation software. Tech. Rep. 943, Dept of Theoretical and Applied Mechanics, University of Illinois at Urbana-Champaign.

Holyer, J. Y. 1983 Double-diffusive interleaving due to horizontal gradients. *J. Fluid Mech.* **137**, 347–362.

Howard, L. N. & Krishnamurti, R. 1986 Large-scale flow in turbulent convection: a mathematical model. *J. Fluid Mech.* **170**, 385–410.

Niino, H. 1986 A linear stability theory of double-diffusive horizontal intrusions in a temperature-salinity front. *J. Fluid Mech.* **171**, 71–100.

Ruddick, B. R., Phillips, O. M. & Turner, J. S. 1999 A laboratory and quantitative model of finite-amplitude intrusions. *Dyn. Atmos. Oceans* **30**, 71–99.

Ruddick, B. R. & Richards, K. 2003 Oceanic thermohaline intrusions. *Prog. Oceanogr.* **56**, 499–527.

Ruddick, B. R. & Turner, J. S. 1979 The vertical lengthscale of double-diffusive intrusions. *Deep-Sea Res.* **26**, 903–913.

Stern, M. E. 1967 Lateral mixing of water masses. *Deep-Sea Res.* **14**, 747–753.

Turner, J. S. 1973 *Buoyancy Effects in Fluids*. Cambridge University Press.

Turner, J. S. & Chen, C. F. 1974 Two-dimensional effects in double-diffusive convection. *J. Fluid Mech.* **63**, 577–592.

https://doi.org/10.1017/S002211200600992X Published online by Cambridge University Press